Drifting Periodic Structures in a Degenerate-Planar Bent-Rod Nematic Liquid Crystal Beyond the Dielectric Inversion Frequency

ARTICLE *in* THE JOURNAL OF PHYSICAL CHEMISTRY B · AUGUST 2008

Impact Factor: 3.3 · DOI: 10.1021/jp804264m · Source: PubMed

5 AUTHORS, INCLUDING:

Pramoda Kumar
Harvard University
15 PUBLICATIONS **122** CITATIONS
SEE PROFILE

Uma Hiremath
Centre for Nano and Soft Matter Sciences
52 PUBLICATIONS **597** CITATIONS
SEE PROFILE

Axel G Rossberg
Queen Mary, University of London
89 PUBLICATIONS **1,052** CITATIONS
SEE PROFILE

K. S. - Krishnamurthy
Centre for Nano and Soft Matter Sciences (…
41 PUBLICATIONS **239** CITATIONS
SEE PROFILE

THE JOURNAL OF PHYSICAL CHEMISTRY B

Letter

Drifting Periodic Structures in a Degenerate-Planar Bent-Rod Nematic Liquid Crystal Beyond the Dielectric Inversion Frequency

Pramoda Kumar, Uma S. Hiremath, C. V. Yelamaggad, Axel G. Rossberg, and K. S. Krishnamurthy

J. Phys. Chem. B, **2008**, 112 (31), 9270-9274 • DOI: 10.1021/jp804264m • Publication Date (Web): 10 July 2008

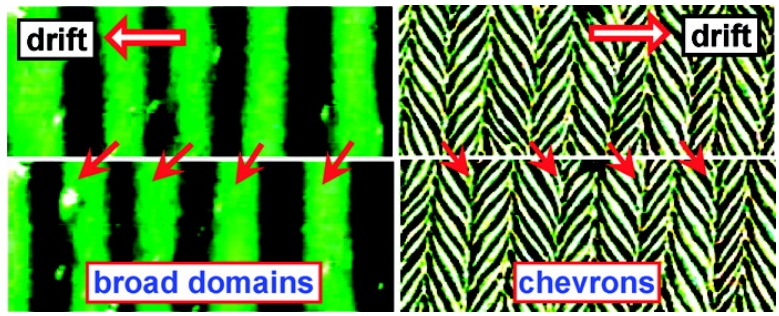

More About This Article

Additional resources and features associated with this article are available within the HTML version:

- Supporting Information
- Access to high resolution figures
- Links to articles and content related to this article
- Copyright permission to reproduce figures and/or text from this article

View the Full Text HTML

The Journal of Physical Chemistry B is published by the American Chemical Society. 1155 Sixteenth Street N.W., Washington, DC 20036

THE JOURNAL OF PHYSICAL CHEMISTRY B LETTERS

2008, *112,* 9270–9274
Published on Web 07/10/2008

Drifting Periodic Structures in a Degenerate-Planar Bent-Rod Nematic Liquid Crystal Beyond the Dielectric Inversion Frequency

Pramoda Kumar,[†] Uma S. Hiremath,[†] C. V. Yelamaggad,[†] Axel G. Rossberg,[‡] and K. S. Krishnamurthy*,[†]

Centre for Liquid Crystal Research, P.O. Box 1329, Jalahalli, Bangalore 560 013, India, and EEP, International Institute for Applied Systems Analysis, 2361 Laxenburg, Austria

Received: May 14, 2008; Revised Manuscript Received: June 13, 2008

We report on the electric-field-generated effects in the nematic phase of a twin mesogen formed of bent-core and calamitic units, aligned homeotropically in the initial ground state and examined beyond the dielectric inversion point. The bend-Freedericksz (BF) state occurring at the primary bifurcation and containing a network of umbilics is metastable; we focus here on the degenerate planar (DP) configuration that establishes itself at the expense of the BF state in the course of an anchoring transition. In the DP regime, normal rolls, broad domains, and chevrons (both defect-mediated and defect-free types) form at various linear defect-sites, in different regions of the frequency–voltage plane. A significant novel aspect common to all these patterned states is the sustained propagative instability, which does not seem explicable on the basis of known driving mechanisms.

Several types of propagative instabilities are known in liquid crystals. In some of these, the dynamics involved is transient, occurring in the process of an energetically more favorable director configuration growing at the expense of a less favorable one. The collapse of a closed Brochard−Leger wall separating two degenerate Freedericksz states of a nematic,[1] motion of domain walls in achiral smectic C (SmC) liquid crystals well above the Freedericksz threshold,[2] and moving wall fronts in the SmC* phase under a d.c. field[3] are some of the instabilities of this kind. Sustained propagation not limited by finite size effects forms a different category of which some examples are the drifting undulations in a SmC liquid crystal,[4] thermo- and electromechanical structural rotations in cholesteric droplets,[5] and the Hopf bifurcation into the traveling roll electroconvective state found in nematic liquid crystals at the Carr−Helfrich (CH) threshold.[6] The last of these effects is of some significance to this study; its origin, which remained challenging for many years, was eventually explained by the weak electrolyte model based on the existence of two mobile ionic species.[6] We have now found a sustained, field-driven drift instability associated with *all* the patterned states evolving beyond the dielectric inversion point, from the degenerate planar configuration of a bent-core nematic; these states include periodic broad-domain and chevron structures formed in the high frequency regime. In this letter we characterize this newly observed instability and discuss the symmetry breaking mechanisms possibly associated with its origin.

The liquid crystal compound used, BCCB, consists of bent-core (BC) and rod-like cyanobiphenyl (CB) mesogenic units linked covalently:

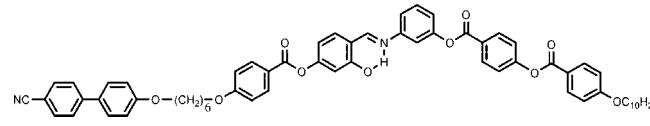

Its phase sequence is reported[7] to be I 162 °C N_b 135.6 °C SmA_b 119.2 °C M 105.5 °C Cr, with I, N_b, SmA_b, M, and Cr denoting isotropic, biaxial nematic, biaxial smectic, uniaxial smectic, and crystal phases, in that order. In our electric field experiments, which concern only the nematic phase, we did not come across any feature that could be ascribed to the conjectured biaxiality. The sample cells were sandwich type, constructed of passivated, indium tin oxide (ITO)-coated glass plates from Delta Technologies. The electrodes were coated with octadecyltriethoxysilane (polyimide) to obtain the homeotropic (planar) orientation. Mylar spacers determined the cell spacing, d, measured interferometrically for thin cells and from cell capacitance for thick cells. The electric field was applied along z, the layer normal. Observations were carried out in transmitted light along z, using a Leitz DMRXP polarizing microscope, equipped with a Mettler hot-stage. The images were recorded using a Sony CCD camera. The voltage source was a Stanford Research Systems DS 345 function generator coupled to a FLC Electronics voltage amplifier (model A800). The applied voltage was measured with a HP 34401A multimeter. For convenience, the polarizer and analyzer with their transmission axes respectively at α and β degrees with respect to x will be represented as P(α)−A(β).

The details of principal permittivities and conductivities in the region of dielectric relaxation are discussed in a separate paper.[8] The data show that the dielectric anisotropy $\epsilon_a = (\epsilon_{||} - \epsilon_{\perp})$, with || and ⊥ being the directions relative to the director $\boldsymbol{n}$, changes sign in the sub-megahertz region from positive to negative as f is increased; for example, at 140 °C, ϵ_a goes to 0

* Corresponding author. E-mail: murthyksk@gmail.com.
† Centre for Liquid Crystal Research.
‡ International Institute for Applied Systems Analysis.

10.1021/jp804264m CCC: $40.75

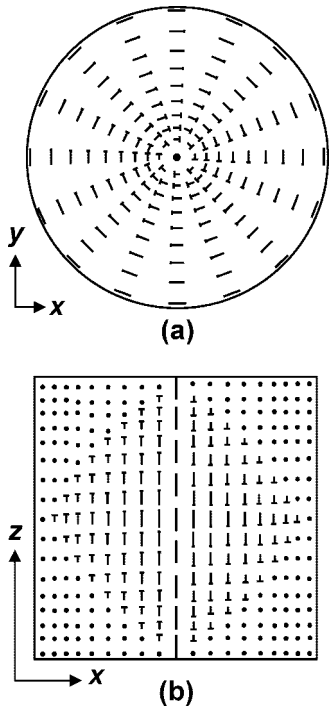

Figure 1. The director field at a +1 defect in the DP state: (a) midplane $z = 0$; (b) vertical section $y = 0$.

at the inversion point $f_i \approx 150$ kHz. The conductivity anisotropy $\sigma_a = (\sigma_{||} - \sigma_\perp)$ remains positive at all frequencies and temperatures; for 140 °C and 150 kHz, $\sigma_{||}$ and $\sigma_\perp$ are 15.9 and 4.7 μS/m, respectively.

Beyond the dielectric isotropy point f_i, the homeotropic sample displays the usual bend-Freedericksz (BF) transition at a well-defined threshold V_F. Optically, this state manifests as a network of alternate +1 and −1 umbilics. As described in our recent report,[8] the BF state (phase 1) is metastable, and an anchoring transition into the DP state (phase 2) occurs through nucleation and front propagation. After the transition to phase 2, the planar substrate alignment enforces structural changes at the earlier umbilical sites; the umbilics transform into linear defects with vertical threads that end in singular points.[9] Figure 1 depicts, for example, the director field corresponding to a +1 defect in the DP state. We have confirmed using a tilt compensator that the local birefringence in the DP state away from the defect cores is about equal to that of a planar monodomain.

On voltage rise, the sequence of bifurcations into patterned states occurring within phase 2 is schematically represented in Figure 2. Broadly, we may distinguish two frequency regimes separated by, say, f_B. Below f_B (∼425 kHz at 140 °C), the first of the patterned states formed is characterized by normal rolls (NRs), with the wave vector along the local easy axis of the director (tangential at +1 sites). Away from the defect core, the corresponding focal lines appear broadly radial at +1 defects and hyperbolic at −1 defects. The periodic pattern for a +1 defect is illustrated in Figure 3a, which is similar to that for a +1 umbilic in phase 1 at lower frequencies (cf. Figure 13, ref 8). In the core region of the defect, shown enlarged in the inset of Figure 3a, the focal lines adopt a spiral geometry; correspondingly, the lines of the director field transverse to the focal lines are also spirals. The radial lines are due to a periodic modulation of the tilt angle θ, which the director makes with its easy axis along a given circle centered on the defect. This is evident from Figure 3b, which demonstrates that, when a single

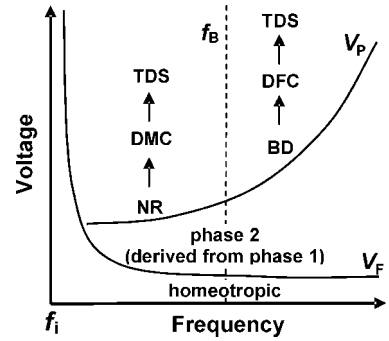

Figure 2. Schematic of the bifurcation states in the conduction regime for phase 2 of BCCB, in the voltage-frequency space, above f_i. V_F and V_P denote the critical voltages for the BF and patterned instabilities, respectively. NR, DMC, BD, DFC, and TDS denote, respectively, the normal roll, defect-mediated chevron, broad domain, defect-free chevron and time-dependent states; f_B is the critical frequency for the onset of BDs.

polarizer is used, focalization occurs markedly for the line images running perpendicular to the electric vector of light and poorly for the lines along the light vector. When the voltage is increased further, edge dislocations begin to nucleate in the periodic structure, as indicated in Figure 3b; the dislocation density rises with the distance from the threshold, and eventually the so-called defect-mediated chevrons (DMCs)[10,11] form. For higher fields, the pattern turns increasingly dynamic, as illustrated in Figure 3c.

The critical voltage for the onset of NRs in phase 2 scales nonlinearly with frequency, as shown in Figure 4. The lower inset presents the critical wavenumber $q = (2d/\lambda)$ as a function of frequency. This variation corresponding to a reduction in the pattern period by a factor of ∼3 over the entire frequency range is of the order expected for the NRs in quasiplanar[12a] and planar[12b] nematics according to the extended CH theory.

For frequencies above f_B, the primary patterned instability manifests optically as nearly periodic broad domains (BDs) as in Figure 5. These bands are best visualized using crossed polarizers suitably oriented, as for example, with P(20)−A(110), the easy axis being parallel to x. The absence of significant focalization by the domains and their appearance at threshold only under crossed polarizers imply an in-plane periodic director modulation. The broad domain mode (BDM) in the nematic phase was observed very early by Trufanov et al.[13] using planarly aligned, highly conducting samples of calamitic liquid crystals such as 4-methoxybenzylindene-4′-butylaniline (MBBA). The BDM in BCCB differs from that in MBBA in some important details. First, the correlated in-plane flows observed with MBBA are not detected in our study. In fact, we found the motion of dust particles to be generally random. Second, the separation between the adjacent dark bands of the pattern is ∼1.5d in MBBA, whereas it is ∼4d in Figure 5. Third, the frequency dependence of the threshold voltage seems stronger in BCCB compared to MBBA. More specifically, as seen in Figure 6, the threshold increases at a rate of ∼0.01 V/kHz between 0.3 and 0.5 MHz in BCCB, but the rate for MBBA of comparable conductivity in the same frequency range (ref 13a, Figure 3, curve 6) is much less.

The BDM in MBBA has been considered[13] to be an anisotropic effect possibly explicable by the extended CH theory that would allow for the finite values of electrical conductivity and the inertial term.[14] The symmetry of the corresponding linear mode (modulations of n normal to the layer plane) is, however, different from the observed distortions of the director field (in-

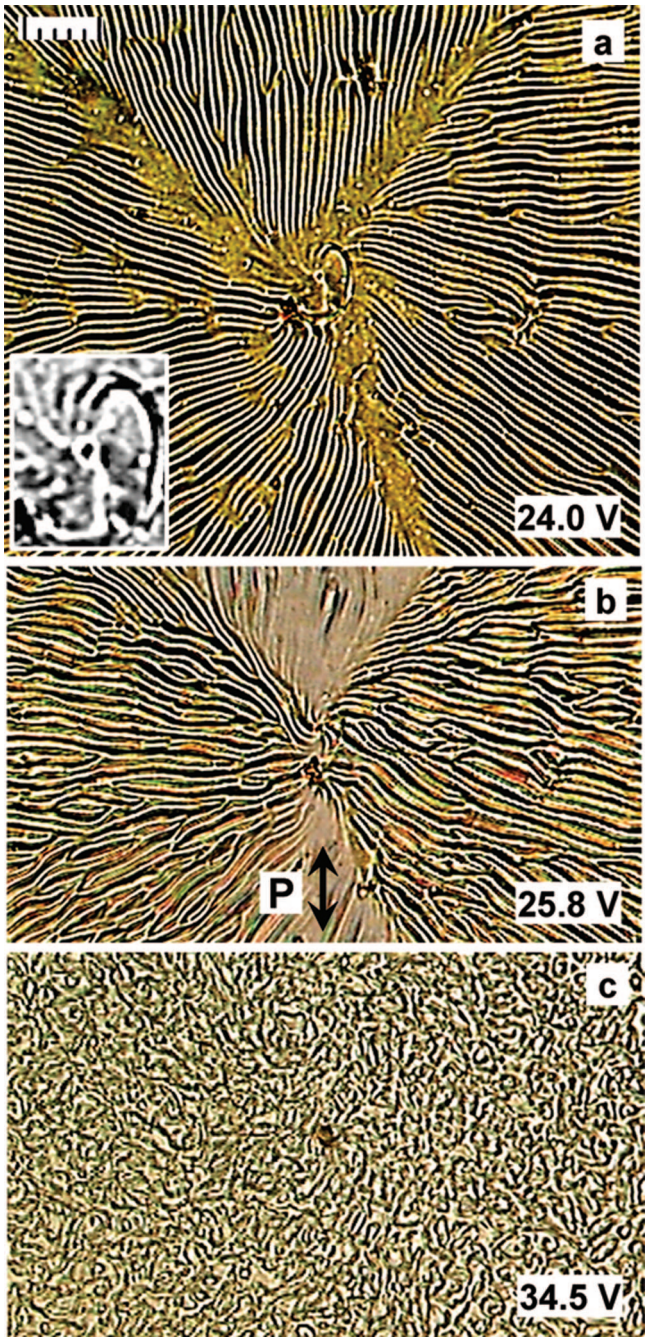

Figure 3. Patterns observed in the same region at 140 °C, 400 kHz. (a) NRs in natural light, characterized, away from the core region, by nearly radial line images, with the wave vector along the director easy axis; virtual plane in focus. The inset is an enlargement of the core region in gray scale to show the spiral-like geometry of the focal lines. (b) NRs with edge dislocations under a single polarizer along y. (c) Time-dependent or quasiturbulent state in natural light; 34.5 V, scale division 10 μm, $d = 19.3$ μm.

plane modulations of n). It is argued that this could be explained by nonlinear effects.[14] However, other mechanisms might need to be considered. For example, it is known[15] that the so-called dynamic flexoelectric effect[16] affects the relaxation behavior of in-plane director modulations. When the coupling constant for the dynamic flexoelectric effect is large and of the right sign, it can, in principle, turn the relaxation dynamics of director modulations into an instability. A more detailed analysis of this mechanism will be presented elsewhere.

At higher fields, broad bands become unstable against the formation of what may be called the defect-free chevrons

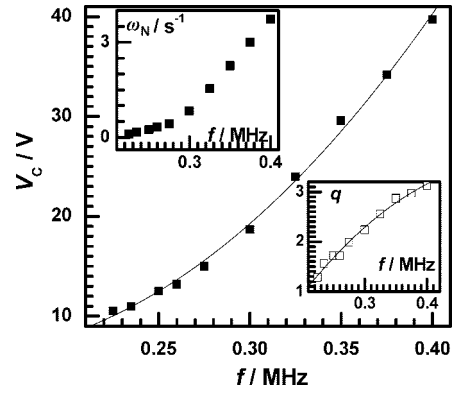

Figure 4. Frequency variation of critical voltage for bifurcation into the NR state in phase 2. The lower inset shows the corresponding frequency variation of critical wavenumber q in units of π/d. The upper inset gives the drift frequency ω_N of the NRs as a function of applied frequency near threshold. 140 °C. $d = 18.9$ μm.

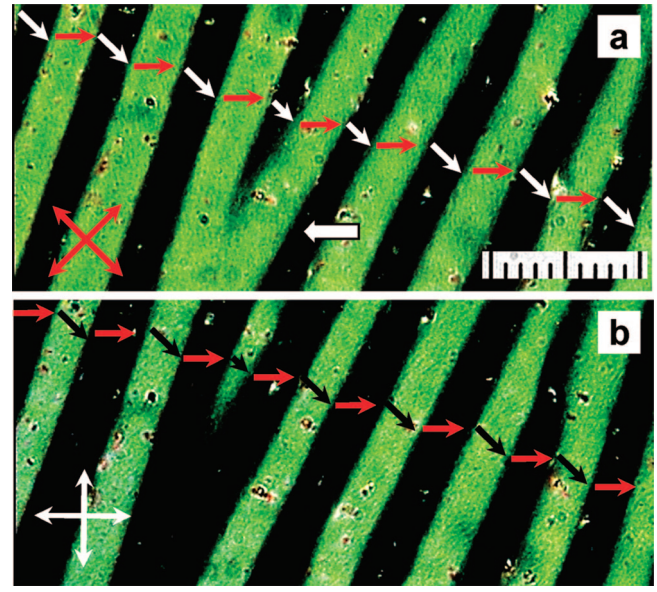

Figure 5. Broad bands formed in the high-frequency regime (above f_B) within the DP state and best seen between crossed polarizers with the incident vibration parallel to the director in one set of alternate bands. The short arrows indicate the director field. P(45)−A(135) in (a) and P(0)−A(0) in (b). The white block arrow shows the drift direction. 135 °C, 200 kHz, 14.4 V. Scale division 10 μm. $d = 14.7$ μm.

(DFCs) following the terminology adopted for similar chevrons in homeotropic samples above the BF transition.[11a]

The central feature of our study is the propagative phenomenon associated with *all* the patterned states belonging to phase 2. The drift occurs right from the onset of the given periodic state. We may first consider the NR state. In Figure 3a, for example, the line images radiating from the defect core drift clockwise (for a video clip, see (i) under Supporting Information, SI). For +1 defects, both clockwise and anticlockwise drifts are observed, but the sense for a given defect remains unchanged with time. For −1 defects, in the NR regime, the hyperbolic lines move inward in one set of opposite quadrants and outward in the other.

We determined the propagation speed of NRs from movie mode recordings of the drifting line images in the virtual plane. From successive images separated in time by 65 ms, we obtained the intensity profiles along a chosen line parallel to the wave vector. A typical map of the profiles is presented in Figure 7.

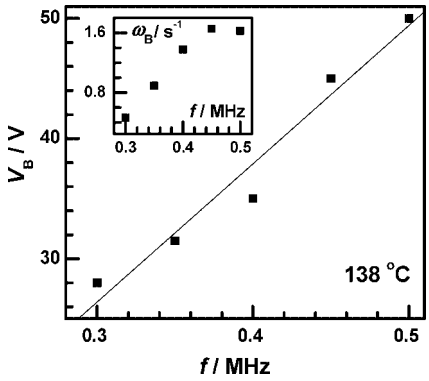

Figure 6. Frequency variation of critical voltage for bifurcation into the BD state in phase 2. The inset gives the drift frequency ω_B of the BDs as a function of applied frequency near threshold. $d = 20.1$ μm.

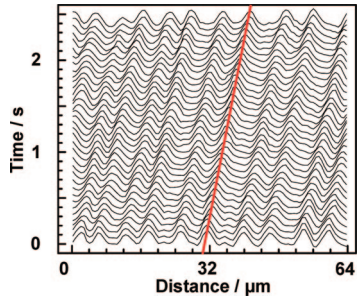

Figure 7. Profiles of transmitted light intensity for the NRs along a fixed line parallel to the wave vector (along x) separated by 0.065 s, plotted successively along the vertical. The pattern of focal lines used is radial, but the chosen intensity-profile region is far from the center where the line-images are largely along y. Virtual plane in focus. The drift speed $\sim$ 4.32 μm/s. The average pattern period $\lambda = 14$ μm. 140 °C. 22.5 V. $d = 19.3$ μm.

The double periodicity of the successive peaks seen here is as expected for the virtual focal lines of the Williams-like roll-pattern.[17] The red line in the figure delineating the locus of constant phase has a slope of $\sim$4.32 μm/s, equal to the average propagative speed, v_P. Interestingly, at a given frequency and voltage, this speed is practically independent of the distance from the defect center. In other words, the pattern rotation seen at a +1 defect site is indicative of a rotation of the structure rather than of any rigid-body-like motion of the local fluid parcel. Second, at a fixed f, v_P is found, from measurements at various voltages up to 15% above the threshold, to be independent of V. The drift frequency $\omega_N = kv_P$ of the NRs, with k as the wavenumber, is a function of f, as illustrated in the upper inset of Figure 4. The nonlinear and continuous increase of ω_N with frequency seen here is similar to the frequency dependence of Hopf frequency of traveling rolls in the usual conduction regime, well below the dielectric relaxation frequency, which is explained by the weak-electrolyte model.[18]

While the traveling nature of NRs may not seem very unusual, that of the BDs (for video clips, see (ii) and (iii) of SI) does appear intriguing. A comparison of panels a and b of Figure 5 shows the leftward shift of the bands. The drift frequency of BDs ω_B increases with f, tending to saturate for very large values of f, as indicated in the inset in Figure 6.

Both DMCs and DFCs display the propagative behavior (for video clips, see (iv) and (v) of SI). This is illustrated in Figure 8 for DMCs obtained through destabilization of NRs at higher voltages.

In order to ascertain whether a planarly aligned monodomain sample would behave in the same way as the one with DP alignment derived through the anchoring transition from the BF state, we examined the BCCB layers held between polyimide-coated, unidirectionally rubbed ITO plates. While the periodic patterns developed in initially planar layers broadly correspond to those in DP layers in different frequency regimes, surprisingly, no drift instability is found with the former. It is, therefore, possible that the anchoring strength is a parameter on which the propagative behavior depends, with weak anchoring promoting the instability. It is also likely that thermal gradients due to dielectric heating are of negligible influence insofar as the drift phenomenon is concerned. In fact, a recent report[19] on heating effects due to dielectric dispersion and ionic conduction shows that, in a nematic layer subject to high frequency fields, even though the sample temperature may rise by several degrees, the temperature gradient across the layer is likely to be very small. It is pertinent to add here that no strict comparison is possible between the instabilities in uniformly planar and DP samples since the two differ in structural symmetry and the drift is quite likely to be symmetry-related, as we discuss below.

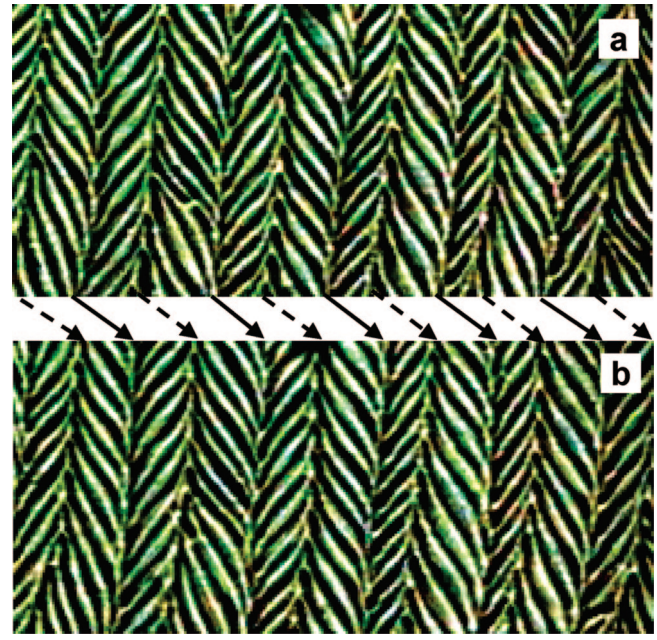

Figure 8. Drifting chevrons obtained through destabilization of NRs. Panels a and b separated by $\sim$22 s are extracted from the video recordings. The slanting arrows between the panels indicate the shift. 200 kHz, 17 V, 135 °C. $d = 14.7$ μm.

What is it that drives the various periodic structures developing from either the BF state[8] or the DP state to travel? We considered several mechanisms to resolve this question, but there does not appear to be a satisfactory explanation yet. In fact, drift of the patterns implies breaking of the symmetry between **c** and $-$**c** in the BF state or the corresponding symmetry in the DP configuration.[20] More precisely, the symmetry is broken in such a way that, when **c** is locally oriented in the x direction, the local system state is neither symmetric under a reflection on the plane normal to the x axis ($x \rightarrow -x$, $y \rightarrow y$, $z \rightarrow z$), nor under a 180° rotation around the y axis ($x \rightarrow -x$, $y \rightarrow y$, $z \rightarrow -z$). While the former symmetry is trivially broken by the BF state, the latter is usually not. In principle, there are three levels of organization at which symmetry-breaking could take place: (a) at the molecular level, (b) macroscopically, at the level of the pattern base state (BF or DP), or (c) by the pattern itself. Case (a) would actually correspond to a ferroelectric phase in which the occurrence of drift independently of the base state (BF or DP) or the patterning mode finds a natural explanation.

Although such a phase is not inconceivable in an asymmetric BC mesogen, it seems too speculative since all known nematics are centrosymmetric. Regarding case (b), symmetry breaking by the pattern base state could be most naturally understood if the top and bottom boundaries were different in some way; this would imply an asymmetry under a flip around the *y* axis (with c || *x*). Differences between the boundaries could be due to imperfections introduced while preparing the sample. However, one would then expect the drift velocity to vary widely between samples, contrary to our observations. It is also conceivable that alignments at the substrates differ for reasons of energy. In that case, the base state spontaneously breaks the symmetry. We should then observe, above the critical voltage, domains with oppositely drifting patterns and, below the critical voltage, sharp walls separating the domains. No indications of the existence of such distinct domains in the base state were found. It is also difficult to visualize such asymmetric configurations for both the BF and DP states in the same experiment.

Case (c) corresponds to a Hopf bifurcation to traveling rolls, which breaks the symmetry spontaneously because rolls traveling in either direction are possible. Such a transition, found for the patterns formed by the CH mechanism in low conductivity nematics, is explained by the so-called weak electrolyte model (WEM).[18] For the NRs in phase 2, considering the dependence of the Hopf frequency on the driving frequency in Figure 4, the WEM may seem quite appropriate, but some questions remain. One is the aforesaid absence of traveling waves in uniformly planar samples. Another is the nonoccurrence of travel in either direction with equal probability; for example, the rotational sense at a given +1 site remains unchanged in time, even though both clockwise and anticlockwise drifts are found between the different +1 sites. Further, the rotational sense at a given site remains unchanged when the field is lowered below the onset and subsequently turned on again. In any case, WEM cannot be applied to the case of BDs, which apparently are not convincingly explained by the CH mechanism.

Most striking, perhaps, is the contrast between observation of drift in the DP state and the absence of any drift in planarly aligned cells. An important difference between the two situations is the presence of numerous linear defects in the DP state, which are absent in the planar cell. Line defects with broken symmetry (Figure 3a) could lead to drifting patterns, and this mechanism is certainly active; all else symmetric, domains will travel around the defects. We would, however, expect this mechanism to be more forceful in the vicinity of defects than far way from them, contrary to our observation that the drift velocity is nearly independent of the distance from the defect core (see (i) of SI).

To summarize this discussion, while there are indications in support of mechanisms at all three levels of organization we considered, none of them seamlessly agrees with all aspects of our observations.

Acknowledgment. We thank Professor K. A. Suresh for his support and encouragement. P.K. is grateful to the Council of Scientific and Industrial Research, India, for a Senior Research Fellowship. K.S.K. and C.V.Y. thank the Department of Science and Technology, India, for an Indo-Bulgarian research project.

Supporting Information Available: Five movie clips of the propagative patterns: (i) NRs as radial domains. First 10 s: polarizer and analyzer axes vertical, $f = 490$ kHz, $V = 22$ V_{rms}, $T = 140$ °C. Next 10 s: natural light, $f = 490$ kHz, $V = 23.5$ V_{rms}, $T = 140$ °C. (ii) BDs and transverse walls, with the latter in focus. Crossed polarizers, $f = 350$ kHz, $V = 40.4$ V_{rms}, $T = 140$ °C. (iii) BDs and transverse walls, with the former in focus. Crossed polarizer and analyzer, with the former at 10° to horizontal. $f = 300$ kHz, $V = 28.1$ V_{rms}, $T = 138$ °C. (iv) DMCs. Single polarizer with its axis horizontal. $f = 200$ kHz, $V = 16.9$ V_{rms}, $T = 135$ °C. (v) DFCs. Polarizer and analyzer axes horizontal. $f = 350$ kHz, $V = 45.5$ V_{rms}, $T = 140$ °C. Horizontal frame-dimension: 420 μm. This material is available free of charge via the Internet at http://pubs.acs.org.

References and Notes

(1) (a) Brochard, F. *J. Phys. (Paris)* **1972**, *33*, 607. (b) Leger, L. *Mol. Cryst. Liq. Cryst.* **1973**, *24*, 45. (c) Krishnamurthy, K. S.; Bhate, M. S. *Mol. Cryst. Liq. Cryst.* **1985**, *128*, 29.

(2) (a) Schiller, P.; Pelzl, G.; Demus, D. *Liq. Cryst.* **1987**, *2*, 21, 131. (b) Stewart, I. W.; Carlsson, T.; Leslie, F. M. *Phys. Rev. E* **1994**, *49*, 2130.

(3) Cladis, P. E.; van Sarloos, W. Some nonlinear problems in anisotropic systems. In *Solitons in Liquid Crystals*; Lam, L., Prost, J., Eds.; Springer-Verlag: New York, 1992; Chapter 4, pp 110−150.

(4) Krishnamurthy, K. S.; Kumar, P. *J. Phys. Chem. B* **2007**, *111*, 2423.

(5) (a) Dequidt, A.; Oswald, P. *Eur. Phys. J. E* **2007**, *24*, 157. (b) Dequidt, A.; Zywocinski, A; Oswald, P. *Eur. Phys. J. E* **2008**, *25*, 217, and references therein.

(6) Dennin, M.; Treiber, M.; Kramer, L.; Ahlers, G.; Cannell, D. S. *Phys. Rev. Lett.* **1996**, *76*, 319.

(7) Yelamaggad, C. V.; Krishna Prasad, S.; Nair, G. G.; Shashikala, I. S.; Shankar Rao, D. S.; Lobo, C. V.; Chandrasekhar, S. *Angew. Chem., Int. Ed.* **2004**, *43*, 3429.

(8) Kumar, P.; Uma, S. H.; Yelamaggad, C. V.; Rossberg, A. G.; Krishnamurthy, K. S. *J. Phys. Chem. B*, in press.

(9) Saupe, A. *Mol. Cryst. Liq. Cryst.* **1973**, *21*, 211.

(10) Rossberg, A. G.; Kramer, L. *Physica D* **1998**, *115*, 19.

(11) (a) Huh, J-H.; Hidaka, Y.; Rossberg, A. G.; Kai, S. *Phys. Rev. E* **2000**, *61*, 2769. (b) Huh, J.-H.; Yusuf, Y.; Hidaka, Y.; Kai, S. *Phys. Rev. E* **2002**, *66*, 031705.

(12) (a) Hertrich, A.; Decker, W.; Pesch, W.; Kramer, L. *J. Phys. II (Paris)* **1992**, *2*, 1915. (b) Bodenschatz, E.; Zimmermann, W.; Kramer, L. *J. Phys. (Paris)* **1988**, *49*, 1875.

(13) (a) Trufanov, A. N.; Blinov, L. M.; Barnik, M. I. *Sov. Phys. JETP* **1980**, *51*, 314. (b) A novel type of the electrohydrodynamic instability in nematic liquid crystals. In *Advances in Liquid Crystal Research and Applications*; Bata, L., Ed.; Pergamon Press: Oxford, 1980; pp 549−560.

(14) Pikin, S. A.; Chigrinov, V. G. *Sov. Phys. JETP* **1980**, *51*, 123.

(15) Rossberg, A. G. The Amplitude Formalism for Pattern-Forming Systems with Spontaneously Broken Isotropy and Some Applications. Dissertation, Universität Bayreuth, 1997. http://www.rossberg.net/ag/dissertation.

(16) Pleiner, H.; Brand, H. R. In *Pattern Formation in Liquid Crystals*; Buka, A., Kramer, L., Eds.; Springer: Berlin, 1996.

(17) Joets, A.; Belaidi, A.; Ribotta, R. *Banach Centre Pub.* **2003**, *62*, 135. and references therein.

(18) Kramer, L. In *Pattern Formation in Liquid Crystals*; Buka, A., Kramer, L., Eds.; Springer: Berlin, 1996.

(19) Yin, Y.; Shiyanovskii, S. V.; Lavrentovich, O. D. *J. Appl. Phys.* **2006**, *100*, 024906.

(20) Here, **c** is the unit vector representing the preferred orientation of the projection of the molecules on the layer plane. It is related to the in-plane director $\mathbf{n}_\perp$ and its amplitude S by $\mathbf{n}_\perp = S(x,y,z)\mathbf{c}(x,y)$. Evidently, **c** and −**c** correspond to opposite director tilts and are not equivalent.

JP804264M